Proceedings of the ASME 2012 International Mechanical Engineering Congress & Exposition
IMECE2012
November 9-15, 2012, Houston, Texas, USA

IMECE2012-86131

ON DYNAMICS OF SPINNING STRUCTURES

K. K. Gupta
NASA – DFRC
Edwards, California, USA

A. Ibrahim*
Norfolk State University
Norfolk, Virginia, USA
aibrahim@odu.edu

ABSTRACT

This paper provides details of developments pertaining to vibration analysis of gyroscopic systems, that involves a finite element structural discretization followed by the solution of the resulting matrix eigenvalue problem by a progressive, accelerated simultaneous iteration technique. Thus Coriolis, centrifugal and geometrical stiffness matrices are derived for shell and line elements, followed by the eigensolution details as well as solution of representative problems that demonstrates the efficacy of the currently developed numerical procedures and tools.

NOMENCLATURE

$\mathbf{C}_C$	Coriolis acceleration matrix
$\mathbf{C}_d$	elastic damping matrix
$\mathbf{K}_E$	elastic stiffness matrix
$\mathbf{K}_G$	geometric stiffness matrix
$\mathbf{K}'$	centripetal acceleration matrix
$\mathbf{M}$	elastic mass or inertia matrix
$\mathbf{N}$	shape function
$\mathbf{f}$	initial force vector
g	aeroelastic or structural damping
i^*	$\sqrt{-1}$, imaginary number
$\mathbf{q}$	displacement vector
$\dot{\mathbf{q}}, \ddot{\mathbf{q}}$	velocity and acceleration vectors
$\mathbf{u}$	displacement vector
ζ	damping
λ	natural frequencies
$\boldsymbol{\lambda}$	structural direction cosine matrix
$\boldsymbol{\varphi}$	structural modes of vibration
$\boldsymbol{\Omega}$	angular velocity matrix, spin rate
ω	frequencies

Superscripts

T	matrix transpose
-1	matrix inverse
e	elementwise

INTRODUCTION

Many practical problems, as turbines, helicopters and others are characterized by rotating components arising out of functional requirements. Others as spacecraft and satellites are often spin stabilized. Their natural frequency analysis [1] is of much importance for subsequent determination of state of stress as well for stability and control analyses. To derive the relevant equations of motion one may consider the elastic deformation $\mathbf{u}_j$ of a point j in a flexible body rotating at a constant angular velocity $\boldsymbol{\Omega}$ about an arbitrary axis, having components Ω_X, Ω_Y, and Ω_Z along the three reference coordinate system axes (Fig. 1). Thus, the position vector may be derived as

$$\mathbf{r} = \mathbf{r}_j + \mathbf{u}_j \tag{1}$$

* Address all correspondence to this author.

whereas the velocity and acceleration vectors can be written as

$$\mathbf{v} = \frac{\partial \mathbf{r}}{\partial t} + \boldsymbol{\Omega} \times \mathbf{r} \tag{2}$$

$$\mathbf{a} = \frac{\partial \mathbf{v}}{\partial t} + \boldsymbol{\Omega} \times \mathbf{v}$$
$$\frac{\partial^2 \mathbf{r}}{\partial t^2} + \dot{\boldsymbol{\Omega}} \times \mathbf{r} + 2\boldsymbol{\Omega} \times \dot{\mathbf{r}} + \boldsymbol{\Omega} \times (\boldsymbol{\Omega} \times \mathbf{r}) \tag{3}$$

respectively; further

$$\boldsymbol{\Omega}\mathbf{r} = \begin{bmatrix} 0 & -\Omega_z & \Omega_y \\ \Omega_z & 0 & -\Omega_x \\ -\Omega_y & \Omega_x & 0 \end{bmatrix} \begin{Bmatrix} r_x \\ r_y \\ r_z \end{Bmatrix} \tag{4}$$

In Eqn. (3), the first term on the right hand side relates to the effects of in-plane stretching on out-of-plane deformation; the second term reduces to zero for steady spin state while the third and fourth terms relate to Coriolis and centripetal acceleration. The preceding equations may be conveniently used in formulating strain and kinetic energies and the governing equation of motion [2] for the entire flexible body may be derived, for the undamped case, using Hamilton's principle as

$$\mathbf{M}\ddot{\mathbf{q}} + 2\mathbf{M}\boldsymbol{\Omega}\dot{\mathbf{q}} + (\mathbf{K}_E + \mathbf{M}\boldsymbol{\Omega}\boldsymbol{\Omega})\mathbf{q} = -\mathbf{M}\boldsymbol{\Omega}\boldsymbol{\Omega}\mathbf{r} \tag{5}$$

or

$$\mathbf{M}\ddot{\mathbf{q}} + \mathbf{C}_C\dot{\mathbf{q}} + (\mathbf{K}_E + \mathbf{K}')\mathbf{q} = \mathbf{f}_c \tag{6}$$

$\mathbf{f}_c$ being the centrifugal force vector and $\mathbf{r}$ representing all $\mathbf{r}_j$, $\mathbf{M}$, $\mathbf{K}_E$, and $\mathbf{K}'$ are respectively the inertia, elastic and centripetal stiffness matrices, $\mathbf{C}_C$ being the Coriolis matrix.

The related analysis starts by first computing the steady-state deflection due to constant spin $\boldsymbol{\Omega}$ by solving

$$(\mathbf{K}_E + \mathbf{K}')\mathbf{q} = \mathbf{f}_c \tag{7}$$

and thereafter calculating the geometrical stiffness matrix $\mathbf{K}_G$ from resulting in-plane stresses. The equation of motion can then be written as below, that also includes damping[2]

$$\mathbf{M}\ddot{\mathbf{q}} + (\mathbf{C}_C + \mathbf{C}_d)\dot{\mathbf{q}} + (\mathbf{K}_E(1 + i^* g) + \mathbf{K}' + \mathbf{K}_G)\mathbf{q} = \mathbf{0} \tag{8}$$

in which $\mathbf{C}_d$ is viscous damping matrix, g is the structural damping parameter, i^* being the imaginary number $\sqrt{-1}$.

To perform relevant dynamic analysis it is essential first to derive expressions for nodal centrifugal forces for various finite elements spinning about an arbitrary axis. Such in-plane forces are used for derivation of k^e_G matrices, where its out-of-plane components are used for developing expression for the element centripetal stiffness matrix k'^e; examples of some of these matrices are derived next.

NUMBERICAL FORMULATION

Derivation of Nodal Centrifugal Forces

Figure 1 shows a typical triangular flat shell element undergoing an uniform spin rate Ω_R along an arbitrary axis.

Using local coordinate system (LCS) defined by x, y, and z axes, the shape function matrix $\mathbf{N}$ for in-plane motion of the element having components along global reference axes X, Y, Z, respectively.

$$\mathbf{u} = \mathbf{N}\mathbf{u}^e \tag{9}$$

where

$$\mathbf{N} = \mathbf{R}\mathbf{Q}^{-1} \tag{10}$$

and in which $\mathbf{u}$ is the displacement vector of a typical point P within the element; $\mathbf{u}^e$ is the element nodal displacement vector, $\mathbf{R}$ is the portion of the shape function matrix having elements that are functions of the local coordinates x and y, and $\mathbf{Q}$ is the portion of the shape function matrix with elements expressed in terms of the element nodal coordinate values. Further defining the internal force vector at any point within the element in the LCS as

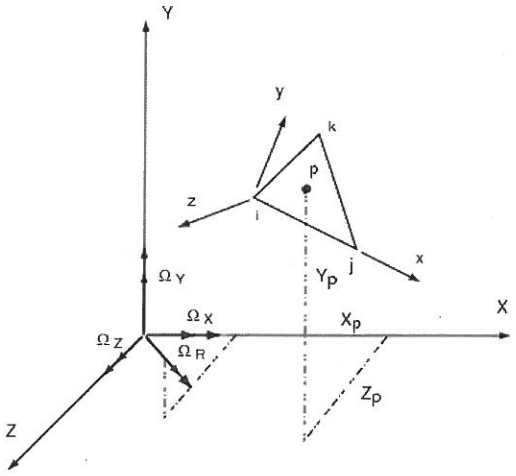

Figure 1 A typical triangular shell element subjected to arbitrary spin rate

$$\mathbf{f} = \begin{bmatrix} f_x & f_y & f_z \end{bmatrix} \tag{11}$$

, the equivalent concentrated nodal forces of a triangular element in the LCS may be expressed as

$$\mathbf{f}^e = \begin{bmatrix} f_{x1} & f_{y1} & f_{z1} & \cdots & f_{x3} & f_{y3} & f_{z3} \end{bmatrix}^T \tag{12}$$

which may also be written in the following form:

$$\mathbf{f}^e = \int_v \mathbf{N}^T \mathbf{f} dv \tag{13}$$

or

$$\mathbf{f}^e = \int_v \mathbf{N}^T \boldsymbol{\lambda} \mathbf{p} dv \tag{14}$$

where $\mathbf{p}$ represents the forces in the global coordinate system at any point within an element, having three components p_X, p_Y, and p_Z in the X, Y, and Z directions, respectively, and $\boldsymbol{\lambda}$ is the element direction cosine matrix:

$$\boldsymbol{\lambda} = \begin{bmatrix} l_x & m_x & n_x \\ l_y & m_y & n_y \\ l_z & m_z & n_z \end{bmatrix} \tag{15}$$

in which $l_x = \cos(X, x)$, and so on. Furthermore, defining X_i, Y_i, and Z_i as the global coordinates of node I of the triangular element, such coordinates for any point within the element may simply be obtained as

$$\begin{bmatrix} X \\ Y \\ Z \end{bmatrix} = \begin{bmatrix} X_i \\ Y_i \\ Z_i \end{bmatrix} + \boldsymbol{\lambda}^T \begin{bmatrix} x \\ y \\ 0 \end{bmatrix} \tag{16}$$

The in-plane element nodal centrifugal forces may next be derived for each of the three components of the spin rate Ω_R which may then be combined to yield the final desired expressions. Thus, typically, corresponding the spin component Ω_X, the appropriate forces are expressed as

$$\mathbf{p} = \rho \Omega_X^2 \begin{bmatrix} 0 \\ Y \\ Z \end{bmatrix} \tag{17}$$

where ρ is the mass density. Upon the employment of the relationships expressed by Eqns. (15) and (16), Eqn. (17) takes the following form:

$$\mathbf{p} = \rho \Omega_X^2 \begin{bmatrix} 0 \\ m_x x + m_y y + Y_i \\ n_x x + n_y y + Z_i \end{bmatrix} \tag{18}$$

Expressions for the element nodal forces is then derived by appropriate substitution of Eqns. (10), (15), and (18) into Eqn. (14), yielding

$$\mathbf{f}_p^e(\Omega_X) = \rho \Omega_x^2 t \left[\mathbf{Q}^{-1}\right]^T \int_0^{y_k} \int_{x_l}^{x_u} \mathbf{R}^T \boldsymbol{\chi} dx dy \tag{19}$$

where t is the element thickness, y_k is the y coordinate of node k, $x_l = x_k y / y_k$ is the lower bound of the x coordinate in the integration process, $x_u = x_j - (x_j - x_k) y / y_k$ is the upper bound of the x coordinate, and

$$\boldsymbol{\chi} = \begin{bmatrix} m_x (m_x x + m_y y + Y_i) + n_x (n_x x + n_y y + Z_i) \\ m_y (m_x x + m_y y + Y_i) + n_y (n_x x + n_y y + Z_i) \end{bmatrix} \tag{20}$$

In Eqn. (19) the vector $\mathbf{f}_p^e$ contains the in-plane element nodal forces in local x and y directions, being expressed as $\begin{bmatrix} f_{x_i} & f_{y_i} & f_{x_j} & f_{y_j} & f_{x_k} & f_{y_k} \end{bmatrix}^T$.

Associate forces due to spin rates in the Y and Z directions may also be similarly expressed as

$$\mathbf{f}_p^e(\Omega_Y) = \rho \Omega_Y^2 t \left[\mathbf{Q}^{-1}\right]^T \int_0^{y_k} \int_{x_l}^{x_u} \mathbf{R}^T \boldsymbol{\gamma} dx dy \tag{21}$$

$$\mathbf{f}_p^e(\Omega_Z) = \rho \Omega_Z^2 t \left[\mathbf{Q}^{-1}\right]^T \int_0^{y_k} \int_{x_l}^{x_u} \mathbf{R}^T \boldsymbol{\xi} dx dy \tag{22}$$

where

$$\boldsymbol{\gamma} = \begin{bmatrix} l_x\left(l_x x + l_y y + X_i\right) + n_x\left(n_x x + n_y y + Z_i\right) \\ l_y\left(l_x x + l_y y + X_i\right) + n_y\left(n_x x + n_y y + Z_i\right) \end{bmatrix} \tag{23}$$

$$\boldsymbol{\xi} = \begin{bmatrix} l_x\left(l_x x + l_y y + X_i\right) + m_x\left(m_x x + m_y y + Z_i\right) \\ l_y\left(l_x x + l_y y + X_i\right) + m_y\left(m_x x + m_y y + Z_i\right) \end{bmatrix} \tag{24}$$

The total element in-plane nodal forces are simply combined as

$$\mathbf{f}_p^e = \mathbf{f}_p^e(\Omega_X) + \mathbf{f}_p^e(\Omega_Y) + \mathbf{f}_p^e(\Omega_Z) \tag{25}$$

and may next be transformed into the global coordinate system (GCS) as

$$\mathbf{p}^e = \boldsymbol{\lambda}^T \mathbf{f}_p^e \tag{26}$$

for subsequent stress analysis and generation of the k_G matrix.

The out-of plane components of an element centrifugal force vector may be derived similarly. Then, the element centrifugal force matrices can be readily formulated as

$$\mathbf{K}'^e(\Omega_X) = \Omega_X^2\left(n_Z^2 + m_Z^2\right)\mathbf{M} \tag{27}$$

$$\mathbf{K}'^e(\Omega_Y) = \Omega_Y^2\left(n_Z^2 + l_Z^2\right)\mathbf{M} \tag{28}$$

$$\mathbf{K}'^e(\Omega_Z) = \Omega_Z^2\left(l_Z^2 + m_Z^2\right)\mathbf{M} \tag{29}$$

$\mathbf{M}$ being the inertia matrix and the complete expression for the global centrifugal force matrix is obtained simply as $\mathbf{K}'^e = \mathbf{K}'^e(\Omega_X) + \mathbf{K}'^e(\Omega_Y) + \mathbf{K}'^e(\Omega_Z)$. For quadrilateral elements, such data as derived from four constituent triangular elements by suitably combining them in an orderly fashion.

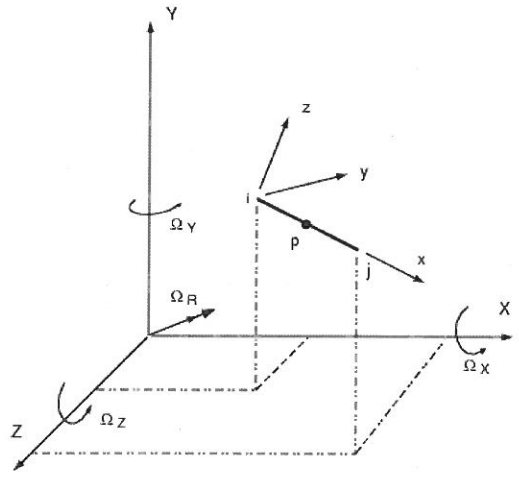

Figure 2 A line element with an arbitrary spin rate

For a line element (Fig. 2), the coordinate at any point within the element is obtained as

$$\begin{bmatrix} X \\ Y \\ Z \end{bmatrix} = \begin{bmatrix} X_i \\ Y_i \\ Z_i \end{bmatrix} + \boldsymbol{\lambda}^T \begin{bmatrix} u_x \\ u_y \\ u_z \end{bmatrix} \tag{30}$$

in which u_y and u_z are deformations at any point on the element in the local y and z directions respectively. Proceeding as in the case of shell elements and assuming nodal lumped masses m, the centrifugal forces at a typical ith node expressed in global coordinate system.

$$p_X^i = m\Omega_Y^2 X_i + m\Omega_Z^2 X_i \tag{31}$$

$$p_Y^i = m\Omega_X^2 Y_i + m\Omega_Z^2 Y_i \tag{32}$$

$$p_Z^i = m\Omega_X^2 Z_i + m\Omega_Y^2 Z_i \tag{33}$$

The element centripetal and geometric stiffness matrices may then be derived as before.

Coriolis Acceleration Matrix

For any structural element such a matrix can be derived as follows

$$\mathbf{C}_C^e = 2\mathbf{M}^e\boldsymbol{\Omega}^e \tag{34}$$

in which the element inertia matrix $\mathbf{M}^e$ in calculated by employing standard formulation

Free Vibration of Spinning Bodies

The associated matrix equation of undamped motion of a flexible spinning body, discretized by the finite element method, can be derived from Eqn. (8) as

$$\mathbf{K}\mathbf{q} + \mathbf{C}\dot{\mathbf{q}} + \mathbf{M}\ddot{\mathbf{q}} = 0 \tag{35}$$

in which $\mathbf{K} = \mathbf{K}_E + \mathbf{K}' + \mathbf{K}_G$ is the stiffness matrix, $\mathbf{C} = \mathbf{C}_C$ the Coriolis force matrix, and $\mathbf{M}$ is the inertia matrix. For small vibration the matrices $\mathbf{K}$ and $\mathbf{M}$ are real, symmetric and positive definite, whereas $\mathbf{C}_C$ is skew symmetric, being also a function of the spin Ω. Eqn. (35) may be resolved into a set of first-order ordinary differential equation as below resulting in a linear eigenvalue problem.

$$\mathbf{A}\mathbf{y} + \mathbf{B}\dot{\mathbf{y}} = \mathbf{0} \tag{36}$$

in which

$$\mathbf{A} = \begin{bmatrix} \mathbf{M} & \mathbf{0} \\ \mathbf{0} & \mathbf{K} \end{bmatrix}, \quad \mathbf{B} = \begin{bmatrix} \mathbf{0} & -\mathbf{M} \\ \mathbf{M} & \mathbf{C} \end{bmatrix}, \quad \mathbf{y} = \begin{bmatrix} \dot{\mathbf{q}} \\ \mathbf{q} \end{bmatrix} \tag{37}$$

The matrices $\mathbf{A}$ and $\mathbf{B}$ are of order $(2\times N)$, N being order of $\mathbf{K}$, $\mathbf{M}$, and $\mathbf{C}$ matrices, noting that $\mathbf{B}$ is skew-symmetric. Solution of Eqn. (36) may be assumed as $\mathbf{y} = \boldsymbol{\varphi} e^{\omega t}$ yielding

$$(\mathbf{A} + \omega\mathbf{B})\boldsymbol{\varphi} = \mathbf{0} \tag{38}$$

where the eigenvalues ω are pure imaginary, the eigenvectors occurring in complex conjugate pairs. Eqn. (38) may be further rearranged [3] as

$$(\mathbf{A} - \lambda\mathbf{F})\boldsymbol{\varphi} = \mathbf{0} \tag{39}$$

in which $\mathbf{F} = i^*\mathbf{B}$ and can also be expressed in expanded form

$$\left(\begin{bmatrix} \mathbf{M} & \mathbf{0} \\ \mathbf{0} & \mathbf{K} \end{bmatrix} - \lambda \begin{bmatrix} \mathbf{0} & i^*\mathbf{M} \\ i^*\mathbf{M} & i^*\mathbf{C} \end{bmatrix} \right) \begin{bmatrix} \dot{\boldsymbol{\Psi}} \\ \boldsymbol{\Psi} \end{bmatrix} = \mathbf{0} \tag{40}$$

where $\mathbf{F}$ is a pure Hermitian matrix, the roots $\lambda = i^*\omega$ are real and occur in pairs λ_1, $-\lambda_1$, ..., λ_N, $-\lambda_N$, associated eigenvectors occurring in complex conjugate pairs. Eigenvalues of the original Eqn. (38) may simply be obtained as λ/i^*, while noting that eigenvectors are the same for both the cases.

Solution of Eqn. (39) has been achieved earlier by various solution techniques [3,4,5]. A variant of the multi-vector progressive iteration technique [6,7,8] is presented next.

Eigensolution by a Progressive multivector Iteration

Equations (38) and (39) are used for the computation of the first NR roots and vectors. Associated solution steps are given next:

Step 1. Perform Cholesky factorization of the real symmetric and positive definite matrix $\mathbf{A}$ of order $2N\times 2N$, taking into account the sparsity of the constituent matrices, initially only,

$$\mathbf{A} = \mathbf{L}\mathbf{D}\mathbf{L}^T \tag{41}$$

$\mathbf{L}$ is an unit lower triangular matrix, $\mathbf{D}$ being diagonal matrix.

Step 2. Form a set of randomly generated $2\times NRT\ (NRT > NR)$ real, trial vectors each of order $2N$, NRT being number of trial vectors.

$$\left[{}^1\hat{\mathbf{x}} \quad {}^1\hat{\mathbf{y}} \quad {}^2\hat{\mathbf{x}} \quad {}^2\hat{\mathbf{y}} \quad \cdots \quad {}^{NRT}\hat{\mathbf{x}} \quad {}^{NRT}\hat{\mathbf{y}} \right] \tag{42}$$

where

$${}^j\hat{\boldsymbol{\varphi}} = {}^j\hat{\mathbf{x}} + i^*\,{}^j\hat{\mathbf{y}}, \quad i^* = \sqrt{-1} \tag{43}$$

Step 3. Initially form

$$\hat{\mathbf{X}}_1 = \left[{}^1\hat{\mathbf{x}}_1 \quad {}^2\hat{\mathbf{x}}_1 \quad \cdots \quad {}^{NRT}\hat{\mathbf{x}}_1 \right] \tag{44}$$

Step 4. Using only unconverged roots, solve

$$\mathbf{A}\mathbf{Y}_{i+1} = \mathbf{B}\hat{\mathbf{X}}_i \tag{45}$$

or in individual matrix form

$$\mathbf{K}\mathbf{Y}_{i+1}^{(l)} = \mathbf{M}\hat{\mathbf{X}}_i^{(u)} + \mathbf{C}\hat{\mathbf{X}}_i^{(l)} \tag{46}$$

yielding $\mathbf{Y}_{i+1}^{(l)}$

$$\mathbf{M}\mathbf{Y}_{i+1}^{(u)} = -\mathbf{M}\hat{\mathbf{X}}_i^{(l)} \tag{47}$$

that is $\mathbf{Y}_{i+1}^{(u)} = -\hat{\mathbf{X}}_i^{(l)}$.

Similarly solve

$$\mathbf{A}\mathbf{X}_{i+1} = \mathbf{B}\mathbf{Y}_{i+1} \tag{48}$$

which can be elaborated as below

$$\mathbf{K}\mathbf{X}_{i+1}^{(l)} = \mathbf{M}\mathbf{Y}_{i+1}^{(u)} + \mathbf{C}\mathbf{Y}_{i+1}^{(l)} \tag{49}$$

yielding $\mathbf{X}_{i+1}^{(l)}$ and also

$$\mathbf{M}\mathbf{X}_{i+1}^{(u)} = -\mathbf{M}\mathbf{Y}_{i+1}^{(l)} \tag{50}$$

from which $\mathbf{X}_{i+1}^{(u)} = -\mathbf{Y}_{i+1}^{(l)}$

In above the superscripts u and l refer the upper and lower half of a vector, respectively.

Step 5. Using unconverged vectors only, perform vector norm check by computing an estimate of the magnitude of a typical vector as

$${}^j\lambda_{i+1} = \left\| {}^j x_i \right\| \Big/ \left\| {}^j x_{i+1} \right\| \tag{51}$$

and check root convergence if $\left({}^j\lambda_{i+1} - {}^j\lambda_i \right) \Big/ {}^j\lambda_{i+1} \le EPSN$, a prescribed convergence parameter. Assuming that first $NR1$ roots have converged, if $NR1 = NR$, proceed to step 8.

Step 6. Setting ${}^1\mathbf{p}={}^1\mathbf{x}$, ${}^2\mathbf{p}={}^1\mathbf{y}$, ${}^3\mathbf{p}={}^2\mathbf{x}$, ${}^4\mathbf{p}={}^2\mathbf{y}, \cdots$, orthonormalize each ${}^j\mathbf{p}_{i+1}$ vector with respect to the $\mathbf{A}$ matrix, only for unconverged $(NR1 - NR)$ vectors, yielding $\hat{\mathbf{p}}$, as follows:

$$\begin{aligned} {}^j\tilde{\mathbf{p}}_{i+1} &= {}^j\mathbf{p}_{i+1} - \sum_{l=1}^{2\times NR1} \left[\left({}^l\mathbf{p} \right)^T \mathbf{A}\, {}^j\mathbf{p}_{i+1} \right] {}^l\mathbf{p} - \\ &\quad \sum_{l=2\times NR1+1}^{j-1} \left[\left({}^l\hat{\mathbf{p}}_{i+1} \right)^T \mathbf{A}\, {}^j\mathbf{p}_{i+1} \right] {}^l\hat{\mathbf{p}}_{i+1} \\ {}^j\hat{\mathbf{p}}_{i+1} &= {}^j\tilde{\mathbf{p}}_{i+1} \Big/ \left[\left({}^j\tilde{\mathbf{p}}_{i+1} \right)^T \mathbf{A}\, {}^j\tilde{\mathbf{p}}_{i+1} \right]^{1/2} \\ & \qquad j = 2\times NR1+1,\ 2\times NRT \end{aligned} \tag{52}$$

Then set back ${}^1\hat{\mathbf{x}}={}^1\hat{\mathbf{p}}$, ${}^1\hat{\mathbf{y}}={}^2\hat{\mathbf{p}}$, ${}^2\hat{\mathbf{x}}={}^3\hat{\mathbf{p}}$, ${}^2\hat{\mathbf{y}}={}^4\hat{\mathbf{p}}$, and so on.

Step 7. Go to step 4 to continue iteration till solution convergence is achieved, in which

$$\hat{\mathbf{X}}_{i+1} = \left[{}^{NR1+1}\hat{\mathbf{x}}_{i+1} \quad {}^{NR1+2}\hat{\mathbf{x}}_{i+1} \quad \cdots \quad {}^{NRT}\hat{\mathbf{x}}_{i+1} \right] \tag{53}$$

Step 8. The Rayleigh-Ritz method, involving only the unconverged roots, is employed next to solve the further reduced eigenvalue problem

$$\hat{\mathbf{A}}_{i+1}\mathbf{Q}_{i+1} = \hat{\mathbf{F}}_{i+1}\mathbf{Q}_{i+1}\hat{\mathbf{\Lambda}} \tag{54}$$

in which

$$\hat{\mathbf{A}}_{i+1} = \overline{\hat{\mathbf{\Phi}}}_{i+1}^T \mathbf{A} \hat{\mathbf{\Phi}}_{i+1}, \quad \hat{\mathbf{F}}_{i+1} = \overline{\hat{\mathbf{\Phi}}}_{i+1}^T \hat{\mathbf{F}} \hat{\mathbf{\Phi}}_{i+1} \tag{55}$$

with

$$\hat{\mathbf{\Phi}}_{i+1} = \left[{}^{NR1+1}\hat{\mathbf{\varphi}}_{i+1} \quad {}^{NR1+2}\hat{\mathbf{\varphi}}_{i+1} \quad \cdots \quad {}^{NRT}\hat{\mathbf{\varphi}}_{i+1} \right] \tag{56}$$

$\hat{\mathbf{\Lambda}}$ being an approximation of $\mathbf{\Lambda}$, the diagonal matrix containing the eigenvalues.

Step 9. A root convergence test is then performed on each unconverged root under consideration,

$$\left| {}^j\hat{\lambda}_{i+1} - {}^j\hat{\lambda}_i \right| \Big/ \left| {}^j\hat{\lambda}_{i+1} \right| \le EPS \tag{57}$$

in which EPS is the root convergence factor.

Step 10. Recompute the eigenvectors,

$$\tilde{\mathbf{\Phi}}_{i+1} = \hat{\mathbf{\Phi}}_{i+1}\mathbf{Q}_{i+1} \tag{58}$$

and relabel $\tilde{\mathbf{\Phi}}_{i+1}$ as $\hat{\mathbf{\Phi}}_{i+1}$ for possible use in step 4 involving $\hat{\mathbf{X}}_{i+1}$ components of $\hat{\mathbf{\Phi}}_{i+1}$.

Step 11. Goto step 4 and perform steps 4, 6, 8-10 only if the number of converged roots $NR1 < NR$. Otherwise go to step 12.

Step 12. End of analysis.

The analysis procedure described herein enables effective computation of the first few roots and vectors which are often the requirement for the important subsequent stability and dynamic response analyses. For further references, steps 4-7, that involves checking root norm convergence, will be referred to as phase 1 operation. Subsequent phase 2 operations, involving Rayleigh-Ritz root convergence calculations consist of step 4, 6, and 8-11. Thus, progressive saving in solution time is obtained in the following key areas. (a) back substitution operation in step 4, (b) vector norm check process in step 5, (c) mass orthonomalization calculation in step 6, (d) Rayleigh Triple matrix multiplication in step 8, (e) Rayleigh vector computation in step 9. It may be noted that all major computations in steps 1-7 are performed in real number thereby saving considerable computational efforts. Solution accuracy factors for $EPSN$, EPS, and $EPSR$ are set to 0.05, 0.00001 and 0.0001, respectively.

NUMBERICAL EXAMPLES

Three example problems are presented next that testifies to the applicability and efficacy of the currently developed solution algorithms for computation of roots and modes of rotating bodies. The first example relates to a spinning cantilever beam subjected to an arbitrary spin rate. Results are presented for both the undamped beam as well as solutions in the presence of viscous and structural damping. The second and third example problems pertain to a rotating cantilever plate, involving rather large degrees of freedom. Solution results and CPU times are compared for the usual and the accelerated version of the associated code.

1. Spinning Cantilever Beam

Figure 3 shows a cantilever beam spinning about an arbitrary axis. Associated data parameters, in consistent British units, are as follows:

Young's modulus, E	=	$30\text{x}10^6$
Cross-sectional area, A	=	1.0
Moment of inertia,		
about y axis	=	1/12
about z axis	=	1/24
Mass density, ρ	=	1/6
Length, L	=	60.0
Scalar nodal viscous damping (in x, y, z translations)	=	0.6283
Structural damping coefficient	=	0.01
Spin rate along Y axis (Ω_Y)	=	0.1 Hz

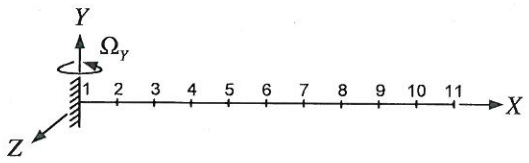

Figure 3 Spinning cantilever beam

Figure 4 depicts the first few mode shapes.

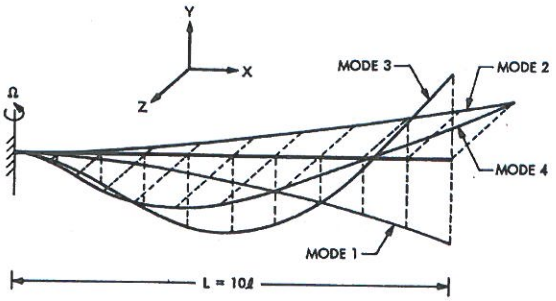

Figure 4 First few mode shapes for a cantilever beam ($\Omega_Y = 0$)

Table 1 lists the natural frequencies of the cantilever beam with various forms of damping.

Table 1 Natural frequencies of a spinning cantilever beam

Mode	Natural frequencies, λ (rad/sec)		
	$\Omega_Y = 0$	$\Omega_Y = 0.6283$ (rad/sec)	
	undamped	undamped	Viscous damping
1	2.6631	± 2.7626	− 0.3799 ± i2.7365
2	3.7660	± 3.7932	− 0.3800 ± i3.7742
3	16.5039	± 16.8409	− 0.3872 ± i16.6360
4	23.3387	± 23.7476	− 0.3870 ± i23.7441
5	45.7488	± 47.0130	− 0.3937 ± i47.0110
6	64.6946	± 66.3958	− 0.3933 ± i66.3944
7	88.7152	± 92.0851	− 0.4012 ± i92.0840
8	125.4547	± 130.0557	− 0.4005 ± i130.0550
9	145.0221	± 152.3365	− 0.4105 ± i152.3357
10	205.0799	± 215.0823	− 0.4093 ± i215.0817

Mode	Natural frequencies, λ (rad/sec)	
	$\Omega_Y = 0.6283$ (rad/sec)	
	Structural damping	Viscous and Structural damping
1	0.0138 + i2.7626 − 0. 0138 − i2.7626	− 0.3659 + i2.7365 − 0.3938 − i2.7365
2	0.0189 + i3.7932 − 0. 0189 − i3.7932	− 0.3608 + i3.7742 − 0.3990 − i3.7742
3	0.0842 + i16.8411 − 0. 0842 − i16.8411	− 0.3030 + i16.6361 − 0.4714 − i16.6361
4	0.1187 + i23.7479 − 0. 1187 − i23.7479	− 0.2682 + i23.7444 − 0.5057 − i23.7444
5	0.2351 + i47.0135 − 0. 2351 − i47.0135	− 0.1585 + i47.0115 − 0.6287 − i47.0115
6	0.3320 + i66.3966 − 0. 3320 − i66.3966	− 0.6130 + i66.3952 − 0.7252 − i66.3952
7	0.4604 + i92.0862 − 0. 4604 − i92.0862	− 0.5922 + i92.0850 − 0.8616 − i92.0850
8	0.6502 + i130.0574 − 0. 6502 − i130.0574	− 0.2497 + i130.0565 − 1.0508 − i130.0565
9	0.7617 + i152.3384 − 0. 7617 − i152.3384	− 0.3512 + i152.3375 − 1.1721 − i152.3375
10	1.0754 + i215.0850 − 1.0754 − i215.0850	− 0.3799 + i215.0843 − 1.4847 − i215.0843

It may be noted that for the undamped spinning cases as well as in the presence of structural damping the roots occur in pairs as $\lambda_1, -\lambda_1, \lambda_2, -\lambda_2, \cdots, \lambda_N, -\lambda_N$, the latter being also complex in nature. For the viscous damping case the roots are in complex conjugate form $(-\alpha \pm i^* \beta)$, whereas when the viscous and structural damping are combined, the real part tends to be somewhat different corresponding to identical imaginary parts, while also noting that the roots of the original set of Eqn. (30) are defined as $\omega = \lambda / i^*$.

Note: lump mass option for non-spinning cases, consistent mass option for spinning cases.

2. Spinning Plate 1

A square plate (Fig. 5), cantilevered at the base is discretized by a 20x20 mesh, and analyses are conducted for spin rates along four sets of local axes (Ω_X, Ω_Y, Ω_Z, and Ω_R). The spin rate along an arbitrary axis, Ω_R (at 45° of each axis) = 100 rad/sec, with an input of Ω_X = Ω_Y = Ω_Z = 57.735 rad/sec; also 100 rad/sec for individual axis spin rates along x, y, and z local axes.. Associated data parameters, in consistent British units, are as follows:

Young's modulus, E	=	10x10^6
Side length, L	=	10.0
Thickness, t	=	0.1
Poisson's ratio, μ	=	0.3
Mass density, ρ	=	0.259 x10^{-3}

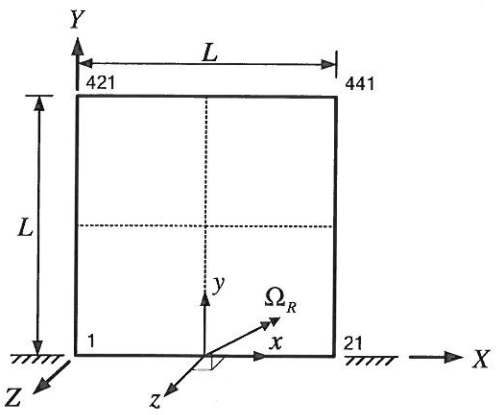

Figure 5 Spinning cantilever plate

Results of these analyses are summarized in Table 2. The first 12 frequencies are given in the table; first few mode shapes are also shown in Fig. 6.

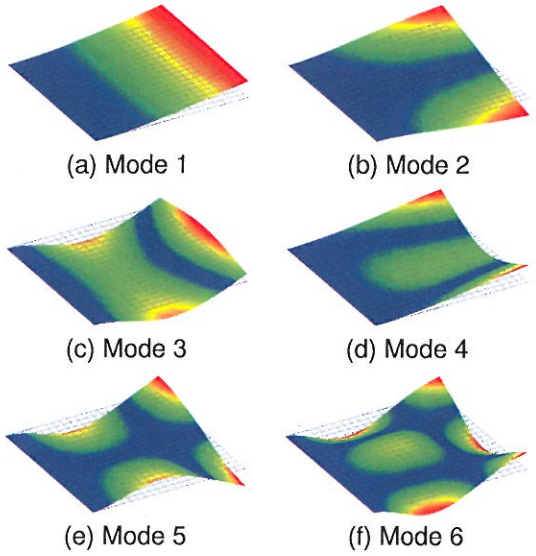

Figure 6 First 6 mode shapes for a cantilever plate ($\Omega = 0$)

Table 2 Natural frequencies (λ in rad/sec) of a spinning cantilever plate (20 x 20) (consistent mass option)

Mode	Non spinning ($\Omega = 0$)	$\Omega_Z = 100$	$\Omega_R = 100$	$\Omega_X = 100$	$\Omega_Y = 100$
1	216.80	245.20	162.02	126.19	51.73
2	529.15	549.78	515.09	497.29	496.24
3	1325.91	1350.84	1331.52	1333.44	1309.70
4	1689.95	1703.87	1690.48	1681.95	1685.67
5	1922.04	1943.08	1928.36	1928.88	1913.21
6	3352.53	3367.97	3358.46	3357.42	3350.10
7	3810.79	3835.60	3823.53	3830.02	3804.62
8	3970.11	3981.71	3974.04	3968.21	3972.17
9	4401.49	4422.87	4412.28	4415.73	4398.49
10	5732.01	5744.32	5737.70	5735.50	5732.96
11	5993.17	6012.35	6003.40	6006.02	5992.21
12	7375.74	7397.47	7388.79	7393.43	7374.15

3. Spinning Plate 2

In an effort to compare the efficacy of the accelerated progressive, process over the original simultaneous iterative technique, another plate (Fig. 7) that results in a rather larger order problem is analyzed next. Associate details of the plate, expressed in British units, are as follows:

Side length, L	=	30.0
FE mesh	=	30 x 30
Spin rate, (Ω_z)	=	100 rad/sec

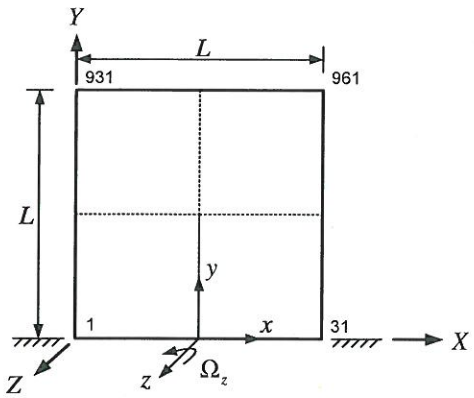

Figure 7 Cantilever plate (30x30) spinning along Z-axis

Other details are as in the previous plate example problem. The results in a 5400 degrees of freedom problem and the relevant eigensolutions are effected using the current progressive simultaneous iterative solution method as well as the original simultaneous iterative solution; this affords a quantitative comparison of the two analysis procedures. Each eigensolution is derived to compute the first 100 modes and roots using 110 randomly generated trial vectors. For both solutions, 8 steps were needed to achieve convergence in phase 1 and another 10 steps were needed in phase 2 to achieve a final solution convergence. Table 3 provides a list of first few frequencies, for both spinning and non-spinning cases.

Table 3 First 20 natural frequencies (λ in rad/sec) of a 30x30 spinning plate (consistent mass option)

Mode	$\Omega = 0$	$\Omega_z = 100$
1	24.1007	109.2439
2	58.9329	131.7314
3	147.6217	210.4748
4	188.3865	310.7209
5	214.3126	347.9099
6	374.5417	414.7329
7	424.7105	519.2821
8	443.5959	573.6855
9	491.2739	647.7871
10	641.6125	734.3848
11	670.5685	816.0489
12	824.2067	902.8594
13	858.9417	961.7461
14	890.9186	997.2900
15	962.1829	1145.9511
16	1033.7367	1180.3106
17	1089.4643	1276.6296
18	1358.6855	1387.4848
19	1377.8232	1440.7086
20	1381.0980	1476.7978

Analyses were conducted for two combinations of progressive features; Table 4 presents relevant details. These data indicates that the progressive method is more efficient than the usual simultaneous iteration technique.

Table 4 Solution details for a 30x30 spinning plate (T: true, F: false for progressive feature)

Computation Phase	PSI[1]	SI[2]
Phase 1	T	F
Phase 2	T	F
Iteration Steps in Phase 1	7	8
Iteration Steps in Phase 2	11	11
CPU time (sec)	78.17	141.79

CONCLUDING REMARKS

The paper presents the novel derivations of constituent Coriolis, centrifugal and geometrical stiffness matrices for various finite elements undergoing rotation along arbitrary axes. This is followed by the matrix formulation of the associated equation of motion, which proves to be convenient for subsequent natural frequency analysis. An accelerated simultaneous iteration solution method is also presented in some details. Finally, a number of example problems are presented for a beam and plates rotating along a set of arbitrary axes, that testifies to the efficacy and broad applicability of the currently developed techniques. A comparison of CPU time is also provided for the current accelerated solution against the original simultaneous iterative method, noting the marked improvement. These techniques were incorporated in a multidisciplinary finite element analysis code [2], capable of solving a large array of practical problems.

ACKNOWLEDGMENTS

We wish to thank Dr. C. L. Lawson for his assistance in the implementation of the eighenproblem solution algorithm.

Thanks are due to S. Choi for his valued assistance in the preparation of this paper.

REFERENCES

[1] Przemieniecki, J. S., 1968, Theory of Matrix Structural Analysis, McGraw-Hill, New York.

[2] Gupta, K. K., and Meek, J. L., 2003, Finite Element Multidisciplinary Analysis, AIAA Education Series, 2nd Edition, Sep.

[3] Gupta, K. K., and Lawson, C. L., 2001, "On a Progressive Simultaneous Iteration Method for Vibration Analysis of Gyroscopic Systems," International Journal for Numerical Methods in Engineering, Vol. 51, pp. 609-617.

[4] Buchau O. A., 1980, "A Solution of the Eigenproblem for Undamped Gyroscopic Systems with the Lanczos Algorithm," International Journal for Numerical Methods in Engineering, Vol. 23, pp. 1705-1713.

[5] Rodrigues J. F. D., Gmuer T. E. C., 1989, "A Subspace Iteration Method for the Eigensolution of Large Undamped Gyroscopic Systems," International

Journal for Numerical Methods in Engineering, Vol. 28, Issue 3, pp. 511-522.

[6] Jennings A. and Orr, D. R. L., 1971, "Application of Simultaneous Iteration Method to Undamped Vibration Problems", International Journal for Numerical Methods in Engineering, Vol. 3, pp. 13-24.

[7] Bathe, K. J. and Wilson, E. L., 1973, "Solution Methods for Eigenvalue Problems in Structural Mechanics International Journal for Numerical Methods in Engineering, Vol. 6, pp. 213-226.

[8] Gupta, K. K., and Lawson, C. L., 1999, "Structural Vibration Analysis by Progressive Simultaneous Iteration Method," Proceeding of the Royal Society of London, Series A: Mathematical and Physical Sciences, Vol. 455, pp. 3415-3424.